Miscibility in Organic/Inorganic Hybrid Nanocomposites Suitable for Microelectronic Applications: Comparison of Modulated Differential Scanning Calorimetry and Fluorescence Spectroscopy

Q. R. Huang,[†,‡] Ho-Cheol Kim,[§] Elbert Huang,[§] David Mecerreyes,[§,⊥] James L. Hedrick,[§] Willi Volksen,[§] Curtis W. Frank,[*,†] and Robert D. Miller[*,§]

Department of Chemical Engineering, Stanford University, Stanford, California 94305; Department of Food Science, Rutgers University, 65 Dudley Road, New Brunswick, New Jersey 08901; and IBM Almaden Research Center, 650 Harry Road, San Jose, California 95120

Received January 9, 2003; Revised Manuscript Received July 29, 2003

ABSTRACT: Modulated differential scanning calorimetry (MDSC) and fluorescence spectroscopy have been used to study the miscibility of methylsilsesquioxane (MSSQ)/poly(methyl methacrylate-*co*-(dimethylamino)ethyl methacrylate) [P(MMA-*co*-DMAEMA)] hybrid nanocomposites, which are promising candidates for spin-on, ultralow dielectric constant materials. MSSQ resins with different initial concentrations of −SiOH (silanol) are used to study the effect of end-group functionality on the phase separation behavior of the hybrid nanocomposites. MDSC measurements, which are useful for studying phenomena with length scales of 10 nm and larger, are consistent with apparent miscibility for P(MMA-*co*-DMAEMA) loading levels as high as 70 wt % for both resins studied. In contrast, fluorescence studies on pyrene-labeled PMMA derivatives, which interrogate substantially smaller distance scales, reveal that pyrene excimer formation occurs at P(MMA-*co*-DMAEMA) loading levels above 6 wt %, thus establishing an upper limit on local miscibility with MSSQ. As the P(MMA-*co*-DMAEMA) loading level increases, the excimer-to-monomer (I_E/I_M) ratio also increases, suggesting that the MSSQ/P(MMA-*co*-DMAEMA) hybrid nanocomposites move toward greater immiscibility. This ratio approaches that of the neat polymer for domain sizes >5 nm as determined by small-angle neutron scattering (SANS). The fluorescence results also show that the lower the initial silanol content in MSSQ, the greater the immiscibility of the MSSQ and porogen, which ultimately translates into larger pores upon porogen burnout, as evidenced by the transmission electron microscopy results.

Introduction

In recent years, considerable research has been devoted to organic/inorganic hybrid nanocomposites.[1] Nanocomposites are defined as materials consisting of two or more components in which the characteristic dimension of one constituent is between 1 and 100 nm. These materials have attracted interest because of their applications in areas such as low dielectric constant films for the microelectronics industry,[2] the preparation of high-surface-area substrates for chemical/biosensors,[3] and usage as catalysts,[4] as gas-separation membranes,[5] and in photonic materials.[6] These nanocomposite materials have elicited interest because of their improved properties relative to the pure polymers, which are often achieved without the sacrifice in density, processability, or toughness that is often observed in conventional composite/blend approaches. One common route to such nanocomposites is through sol−gel polymerization which is based on the hydrolysis and condensation of various silicate precursors such as metal halides and alkoxides to form an interconnected three-dimensional network.[7]

Hybrid nanocomposites can serve as precursors to porous low-*k* insulators used to mitigate the signal delays caused by capacitive coupling and crosstalk in the back-end-of-the-line (BEOL) interconnect wiring as microelectronic feature sizes decrease to sub-150 nm and wiring densities increase.[8] We are particularly interested in nanocomposites produced by cross-linking of sol−gel organosilicates in the presence of sacrificial organic macromolecules because the nanoporous films subsequently generated represent promising candidates for spin-on ultralow dielectric constant (ULK) materials.[2] The nature of the local environment within a porous film is important for ultralow-*k* applications. For example, current chip manufacturing processes require the cured nanoporous materials to be hydrophobic to avoid moisture adsorption, and the average pore sizes should be 15 nm or less in diameter, considerably smaller than minimum dimensions for current high-performance devices. Ideally, closed-cell pores are preferred to optimize mechanical properties and to avoid environmental contamination and inadvertent electrical contact during integration. If the polymer thermal degradation temperature occurs after the point where the maximum rigidity of the organosilicates is achieved, pore collapse will be minimized and the final pore sizes will be similar to those of the polymer domains prior to burnout.

The polymer domain sizes in hybrid nanocomposites depend on, among other things, the degree of mixing prior to and after matrix cross-linking. The need to understand the polymer−organosilicate miscibility and the nature of the local environments within a nanocomposite requires techniques that are sensitive at low concentrations and nanosize scales. Fluorescence spectroscopy becomes a method of choice due to its convenience and intrinsic sensitivity.[9] Although a number of

[†] Stanford University.
[‡] Rutgers University.
[§] IBM Almaden Research Center.
[⊥] Current address: New Materials Department, Center for Research and Development in Electrochemistry (CIDETEC), Paseo Mikeletegi 61-1, E-20009, San Sebastián, Spain.
* To whom all correspondence should be addressed.

10.1021/ma034034d CCC: $25.00
Published on Web 09/12/2003

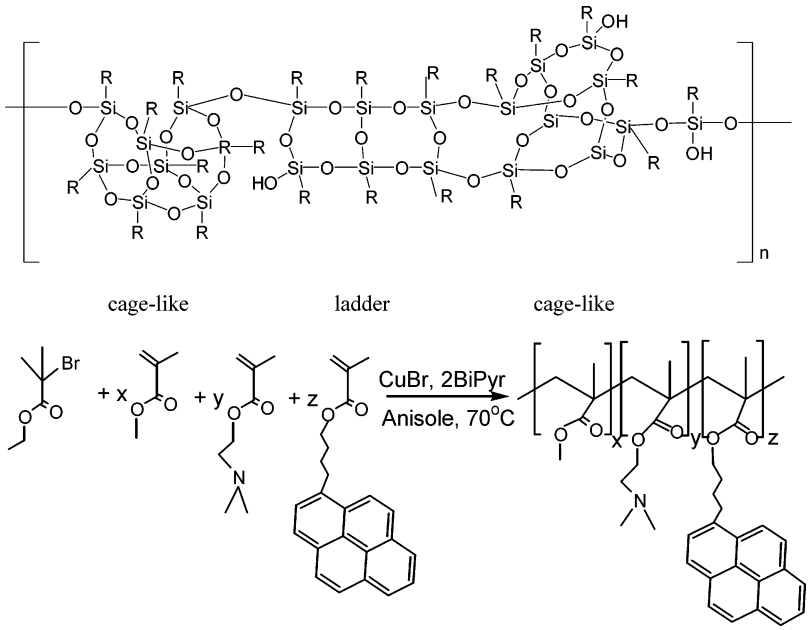

Figure 1. (a, top) Representative types of molecular structures in methylsilsesquioxane (MSSQ). (b, bottom) Synthesis of pyrene-labeled P(MMA-*co*-DMAEMA) by atom transfer radical polymerization (ATRP).

different analytical techniques, such as solid-state NMR,[10] small-angle neutron scattering,[11a,b] small-angle X-ray scattering,[11c,d] differential scanning calorimetry,[12] dynamic mechanical analysis (DMA),[13] and dielectric spectroscopy,[14] can also yield information on the structure and morphology of the nanocomposites, they generally require concentrations of the minor component to exceed 5%. Fluorescence spectroscopy shows potential in overcoming this disadvantage and can provide both high sensitivity at low concentrations and interrogate local microenvironments.

In a previous study,[15] poly(methyl methacrylate-*co*-(dimethylamino)ethyl methacrylate) [P(MMA-*co*-DMAEMA)] was used as a sacrificial porogen to produce nanoporous methylsilsesquioxane (MSSQ) with ultralow dielectric constants ($k < 2.0$) and superior film quality. The initial miscibility between MSSQ and P(MMA-*co*-DMAEMA) is promoted by strong hydrogen-bonding interactions between −SiOH end groups in MSSQ before cross-linking and the tertiary amino substituent in P(MMA-*co*-DMAEMA). The objective of this paper is to develop a molecular-level understanding of the polymer−polymer miscibility and phase separation occurring in MSSQ/P(MMA-*co*-DMAEMA) hybrid nanocomposites. Toward this goal, we have incorporated a fluorescent pyrene substituent into some of the methacrylate side chains. Pyrene is a frequently used chromophore in fluorescence studies of labeled polymers.[16] It was selected as the molecular-level probe because it has a long singlet lifetime and readily forms excimers.[9a] Previous work on polymer blends has demonstrated that excimer fluorescence studies can detect phase separation that occurs on a scale too small to be noticed visually.[17] In addition, the vibronic structure of the pyrene emission is sensitive to the local environment surrounding the pyrene molecules.[18] Compared with traditional methods such as differential scanning calorimetry (DSC), which is limited in sensitivity and is usually applicable to polymer domain sizes >10 nm, excimer fluorescence is sensitive to substantially smaller polymer domains (i.e., ∼1 nm). However, excimer fluorescence is less sensitive to changes in domain sizes as they grow larger and approach macrophase-separated systems.[17] The formation of larger domains is usually manifested by the appearance of separate T_g's for the components revealed in MDSC curves. Since MDSC and excimer fluorescence provide data that are complementary to each other, in this paper we describe the use of both in studies on MSSQ/polymer nanohybrids.

Experimental Section

Materials. Methylsilsesquioxane (MSSQ) prepolymer samples (see Figure 1a) from two separate manufacturers were examined. MSSQ-HI ($M_n = 1816$; $M_w/M_n = 3.46$) and MSSQ-LO ($M_n = 1625$; $M_w/M_n = 5.65$) have similar molecular weights, as determined by gel permeation chromatography (GPC), and are distinguished primarily by the amount of silanol (Si−OH) present in the uncured samples.[15] The designations MSSQ-HI and MSSQ-LO refer to resins with larger or smaller amounts of silanol groups, respectively. The former was obtained from Techniglas (GR-650F) while the latter was produced by Dow Corning. The solvent propylene glycol methyl ether (PMOH, 98+%) was purchased from Aldrich Chemical Co. (Milwaukee, WI) and used as received.

^{1}H NMR Measurements. ^{1}H NMR spectra were recorded in chloroform-*d* solution using a Bruker AM 250 spectrometer operating at 250 MHz.

Gel Permeation Chromatography. GPC analyses were performed in THF on a Waters home-assembled chromatograph consisting of a Waters 717 autosampler, a 515 HPLC pump with a Waters 410 differential refractometer, and a Waters 996 photodiode array detector equipped with four 5 μm Waters columns (300 × 7.7 mm) connected in series, each with successively increasing pore sizes (100, 1000, 100 000, 1 000 000 Å). The P(MMA-*co*-DMAEMA) and MSSQ molecular weights were calculated relative to linear polystyrene standards.

Sample Preparation. Samples for fluorescence measurements were prepared as follows: solutions of MSSQ and py-P(MMA-*co*-DMAEMA) in PMOH (20 wt % solids) were loaded into a disposable syringe and filtered through a 0.2 μm Millex PTFE filter (Millipore, Inc.) directly onto a clean single-polished ⟨100⟩ prime Si wafer. The coated substrate was spun at 3000 rpm for 30 s. Each sample was heated at 3 °C/min under argon to a desired set temperature and held for 2 h before cooling. The final film thicknesses ranged from 0.6 to 0.9 μm, depending on porogen loading. MDSC samples were

coated on glass microfiber filters (Whatman), dried in a vacuum oven at 80 °C overnight, and then heated at 3 °C/min under argon to 180 °C and held there for 2 h.

Characterization of Pyrene-Labeled P(MMA-*co*-DMAEMA). The relative composition of MMA, DMAEMA, and 4-(1′-pyrenebutyl) methacrylate in the pyrene-labeled P(MMA-*co*-DMAEMA) was determined by integration of the ^{1}H NMR spectrum (see Supporting Information). These ^{1}H NMR studies indicated that the py-P(MMA-*co*-DMAEMA) copolymer contained ~3 mol % pyrene-tagged MMA, 29 mol % DMAEMA, and 68 mol % MMA, values that match very closely the feed composition. Since the purity of the py-P(MMA-*co*-DMAEMA) was important, we established that the pyrene groups were covalently attached to the polymer through the use of both UV−vis and refractive index (RI) detectors in the GPC analysis (see Supporting Information). The elution curves for both the UV−vis (λ = 340 nm) and RI detectors peak at the same elution time. The molecular weight of the py-P(MMA-*co*-DMAEMA) determined by GPC is M_n = 8700 g/mol, and the polydispersity was relatively narrow (M_w/M_n = 1.26), as expected for controlled ATRP.

Dynamic Mechanical Analysis (DMA). DMA measurements were recorded using a DMA 983 dynamic mechanical analyzer (TA Instruments) with an oscillation frequency of 1 Hz. Temperature scans were recorded at a ramp rate of 3 °C/min from 25 to 500 °C under nitrogen flow.

Modulated Differential Scanning Calorimetry (MDSC). MDSC is a variation of DSC that allows the differentiation of overlapping transitions. Depending on the underlying heating rate, period, and amplitude of modulation, the technique can provide improved resolution and sensitivity over conventional DSC.[19] MDSC studies were carried out using a TA 2920 (TA Instruments) with a two-point calibration using indium and tin under nitrogen purge. Temperature scans were performed at 4 °C/min from 25 to 200 °C for the hybrid nanocomposites and from 25 to 300 °C for the neat resins.

Fluorescence Measurements. The emission and excitation spectra of the hybrid nanocomposites were measured using a fluorescence spectrometer (FS 900CDT spectrometer, Edinburgh Instruments) with a 450 W steady-state xenon arc lamp. Films were excited in a front-face arrangement to minimize self-absorption. All spectra were taken with 0.5 mm slit widths and 0.5 s dwell time. The excitation wavelength used for the pyrene emission spectra was 343 nm, corresponding to the ^1L_a band of the pyrene ring. The sample chamber was purged with nitrogen for all measurements to prevent photooxidation effects.

Transmission Electron Microscopy (TEM). TEM samples were prepared using a fei 830XL focused ion beam instrument. The samples were observed using a TopCon-002B transmission electron microscope.

Results

Modulated Differential Scanning Calorimetry (MDSC) Analysis. The morphology of the hybrid nanocomposites is largely determined by resin structure and the processing conditions (e.g., cure temperature and porogen loading). The best morphological model system for the final porous structure is the fully cross-linked hybrid nanocomposite in which porogen polymers phase separate, lose their diffusional mobility, and are confined within the organosilicate matrix. In-situ structural evolution studies using small-angle neutron scattering (SANS) with partially deuterated P(MMA-*co*-DMAEMA) indicate that the microphase-separated domains of P(MMA-*co*-DMAEMA) in the nanohybrid and the pore sizes ultimately generated by thermal decomposition of porogen are practically identical.[11a] To determine suitable processing conditions, we performed modulated differential scanning calorimetry (MDSC) measurements.

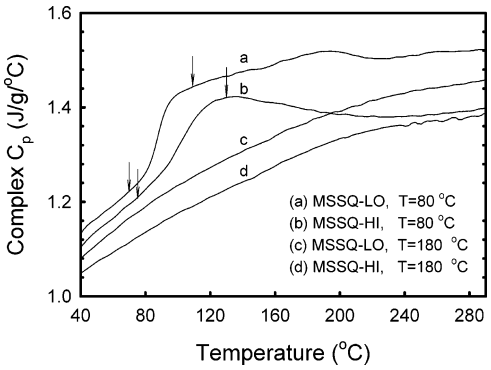

Figure 2. MDSC results of MSSQ-HI and MSSQ-LO neat resins cured at different temperatures: (a) MSSQ-LO at 80 °C, (b) MSSQ-HI at 80 °C, (c) MSSQ-LO at 180 °C, and (d) MSSQ-HI at 180 °C.

This technique, which requires minimal sample preparation, provides both qualitative and quantitative information on physical and chemical changes involving endothermic or exothermic processes and/or changes in heat capacity. It has been used to determine the miscibility of polymer blends through the measurements of glass transition temperature (T_g) since each glass transition reflects a distinct segmental relaxation environment.[20] The existence of a single, composition-dependent T_g in a blend indicates molecular homogeneity on a scale of about 10−30 nm, while multiple T_g's reflect macrophase separation or partial miscibility of the blend components.[21] Figure 2 shows the MDSC results on neat MSSQ-HI and MSSQ-LO resins cured at two different temperatures: (a) MSSQ-LO cured at 80 °C, (b) MSSQ-HI cured at 80 °C, (c) MSSQ-LO cured at 180 °C, and (d) MSSQ-HI cured at 180 °C. A number of conclusions can be drawn from Figure 2. First, although MSSQ-HI and MSSQ-LO have similar molecular weights by GPC, the T_g value of MSSQ-HI heated to 80 °C (solvent removal) is higher (T_g = 111 °C) than that of MSSQ-LO (T_g = 88 °C) similarly cured. This is presumably due to the higher concentration of hydrogen bonding end groups (−SiOH) present in MSSQ-HI. The thermal curves for the samples cured at 80 °C (a and b) also suggest a higher cross-linking temperature for MSSQ-LO (~180 °C) than MSSQ-HI (~130 °C), as evidenced by the respective drop in heat capacities. Second, the segmental mobility of both MSSQ-HI and MSSQ-LO is nearly lost, and significant chain extension and/or cross-linking occurs by 180 °C, as evidenced by the disappearance of the distinct glass transition temperatures for both resins. Thus, the morphology of the resulting hybrid nanocomposites should be locked in at temperatures ≥180 °C. This has been further verified by in-situ temperature-dependent SANS studies on MSSQ-LO using the partially deuterated porogen.[11a] The neutron scattering intensity varies as a function of curing temperature, and strong and constant scattering intensities were observed for the samples heated above 125 °C, indicating that the phase separation takes place and the porogen phase is locked in the MSSQ matrix. The porogen domain size of the hybrid nanocomposites heated above 125 °C is almost identical to the pore size ultimately generated by further heating. The SANS data suggest that the final pore size is determined by the phase-separated domain size of hybrids that is governed by the interaction between MSSQ and porogen.

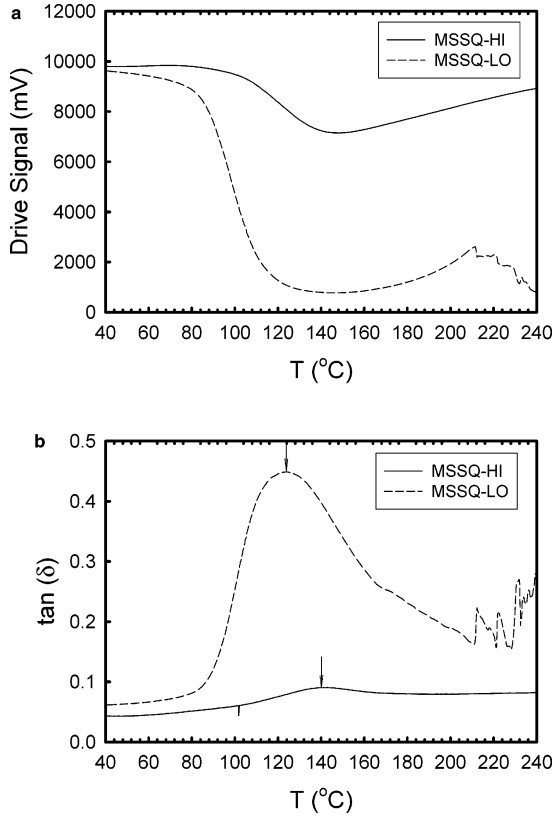

Figure 3. Dynamic mechanical analysis (DMA) results of MSSQ-HI (solid line) and MSSQ-LO (dashed line) cured at 80 °C. The drive signal is directly related to shear storage modulus.

The dynamic mechanical analysis (DMA) data shown in Figure 3 suggest that MSSQ-HI initially heated to 80 °C shows a lower modulus drop at T_g than MSSQ-LO similarly treated. This is at least partially due to the fact that MSSQ-HI undergoes cross-linking in the temperature region 130−160 °C, while the cross-linking of MSSQ-LO begins at higher temperatures (∼180 °C, Figure 2). The relative changes in modulii at T_g are meaningful here since the measured drive signals for both samples after solvent removal are comparable. In addition, the lower segmental mobility for MSSQ-HI heated to 80 °C is manifested by the higher value of T_g and broader nature of the transition as evidenced by Figure 3b. The thermal stability of the P(MMA-*co*-DMAEMA) porogen is also important, and for the study of nanohybrids the maximum processing temperature should be lower than the porogen degradation temperature. Since P(MMA-*co*-DMAEMA) starts to partially thermally degrade at temperatures above 200 °C,[15] we limit the upper cure temperature for the hybrid nanocomposites to $T \leq 180$ °C.

The MDSC data for the hybrids heated to either 80 or 180 °C are shown in Figures 4−7. The lower temperature is sufficient to remove solvent without initiating significant cross-linking. The glass transition temperature T_g is defined as the midpoint between the arrows designating the deviation from the low- and high-temperature heat capacity slopes. For the samples cured at 80 °C, at least three features are apparent, as shown in Figures 4 and 5. First, at 20 wt % loading, the T_g's of the hybrids for both resins are somewhat higher than those of either the individual neat resin or the polymer (T_g = 84 °C). Detailed analysis is complicated since it is known that amines can accelerate the curing of MSSQ resins.[22] Second, a single composition-dependent T_g, which shifts to lower temperatures with increasing polymer loading, is found in all cases. The observation of a single T_g is consistent with apparent miscibility between the MSSQ resins and P(MMA-*co*-DMAEMA) cured at low temperatures, although the similarities in the T_g's between the polymer and the resins make the resolution of the component values difficult. Finally, in the second run (after heating first to 200 °C) for the 20 wt % polymer samples, the MDSC curves for both hybrid nanocomposites are broader, and the distinct glass transition temperature largely disappears. Since we know from SANS studies that curing to 200 °C causes phase separation, the failure to observe a T_g suggests that either the domains are too small to observe by DSC or the porogen concentration is too low. Similarly, the T_g's for both neat resins cured at 180 °C disappear because of extensive cross-linking, as shown in Figure 2.

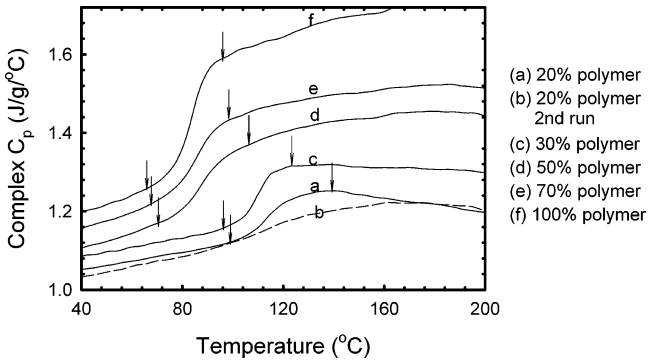

Figure 4. MSSQ-LO/P(MMA-*co*-DMAEMA) nanocomposites cured at 80 °C.

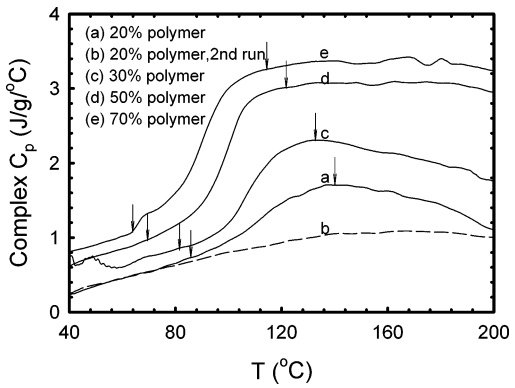

Figure 5. MSSQ-HI/P(MMA-*co*-DMAEMA) nanocomposites cured at 80 °C.

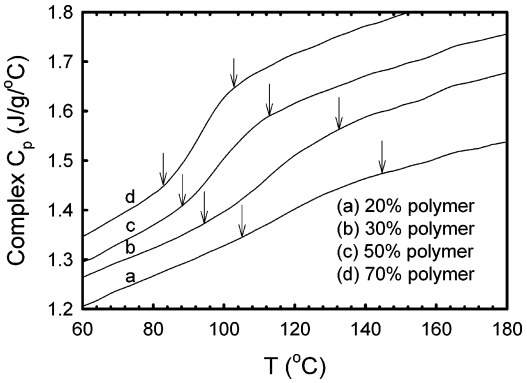

Figure 6. MSSQ-LO/P(MMA-*co*-DMAEMA) nanocomposites cured at 180 °C.

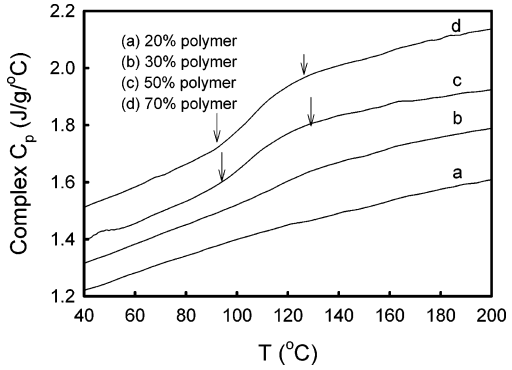

Figure 7. MSSQ-HI/P(MMA-*co*-DMAEMA) nanocomposites cured at 180 °C.

The T_g of the 20 wt % MSSQ-HI hybrid cured at 80 °C (Figure 5) is similar to that of the pure resin (112 vs 111 °C) and progressively decreases with porogen loading, approaching that of the pure porogen (88 vs 83 °C) at 70 wt % loading. However, the measured T_g's for both 20 and 30 wt % MSSQ-LO nanocomposites similarly cured (Figure 4) are significantly higher than either of the pure components. The higher values of T_g for the 20 and 30 wt % MSSQ-LO hybrids remain an interesting puzzle. One possibility is that the low hydroxyl endgroup content of MSSQ-LO selectively interacts with the amino substituents on the porogen, restricting the mobility of both porogen and resin. This effect would quickly saturate with loading, resulting in a T_g value that moves toward that of the pure porogen. In the case of the MSSQ-HI hybrids which contain a larger number of hydrogen-bound −SiOH end groups, the interaction of a few with the amino substituents of the porogen would have less effect since the abundant end groups are expected to be hydrogen bound anyway.

Figures 6 and 7 show the corresponding MDSC results for nanocomposites formed from P(MMA-*co*-DMAEMA) with MSSQ-LO and MSSQ-HI cured at $T = 180$ °C. Similar to Figures 4 and 5, again only a single T_g is observed in the nanocomposites, except that the respective MDSC curve inflections (loading levels >20 wt %) shift to higher temperatures and are broader. Here we note that a distinct T_g is not observed for either neat resin cured to 180 °C (see Figure 2). However, the behaviors of the MSSQ-HI and MSSQ-LO hybrids cured to 180 °C are clearly different in two ways: (1) T_g of the MSSQ-HI hybrid (Figure 7) appears at a slightly higher temperature than that of MSSQ-LO sample (Figure 6) of the same composition, which may indicate stronger interactions of P(MMA-*co*-DMAEMA) with the former resin and/or the formation of smaller domains; (2) the MDSC curves for the MSSQ-HI samples show an obvious glass transition temperature only at porogen loadings higher than 30 wt %. In contrast, the hybrids of MSSQ-LO show a detectable glass transition temperatures even at porogen loading levels as low as 20 wt %. Such an effect could be consistent with the formation of smaller domains in the former which increase in size with porogen loading, as demonstrated by the recent SANS studies using partially deuterated porogen (30 and 50 wt %).[11b] The SANS data also show that, for a given porogen loading level, the domain size is larger for the MSSQ-LO samples. SANS results show substantial scattering intensities for both MSSQ hybrids cured at 180 °C, although the absolute scattering intensities from the MSSQ-LO samples are much greater than those from the MSSQ-HI hybrids. No significant scattering intensity was observed for either hybrid cured at 80 °C, which indicates phase-mixed structures.

In summary, the MDSC results show only a single observable T_g in all the hybrid nanocomposites studied. In principle, this is consistent with either miscibility between P(MMA-*co*-DMAEMA) and MSSQ or the formation of polymer domain sizes that are too small to be detected by DSC analysis. For curing at 180 °C, no T_g is expected for the cross-linked matrix, and any observed glass transition temperature must be associated with the polymer-rich phase since SANS experiments indicate appreciable phase separation at this temperature. In addition, the MDSC technique is especially insensitive to the morphology of cured hybrid nanocomposites with ≤20 wt % P(MMA-*co*-DMAEMA). The quantitative interpretation of the MDSC results for the MSSQ/P(DMAEMA-*co*-MMA) systems is very complicated. At low cure temperatures (e.g., 80 °C) before significant cross-linking has occurred, the T_g value of MSSQ-LO (88 °C) is relatively close to that of the pure porogen (83 °C). This assumes that the presence of the amino-containing porogen does not further advance the cross-linking level upon solvent removal at 80 °C. The similarities of the T_g's for both resins and porogen raise the question of whether each individual T_g could be resolved by MDSC even if phase separation into domains of high purity was occurring. This situation would be further exacerbated if the phase separation produced mixed purity domains. Considering these caveats, we make the following observations for the samples cured to 80 °C. For the MSSQ-LO mixtures, T_g values were observed even for low loading levels (20 and 30 wt %), but these were substantially higher than either of the pure components. Beyond 30 wt %, the change in the complex C_p increases and the T_g value approaches that of the pure porogen (see Figure 4). The higher values measured for 20 and 30 wt % loading could originate from strong interactions between the polymer and matrix (as either a miscible blend or a phase-separated system with small domains). These interactions apparently saturate at higher loading levels, causing a T_g closer to that of the polymer and/or the resins.

A similar trend is observed for the MSSQ-HI blends (Figure 5) also cured to 80 °C, except that no distinct T_g was observed for porogen concentrations below 30 wt %. Above 30 wt %, the system behaves qualitatively similar to the MSSQ-LO nanocomposites with the measured T_g moving to lower values as the loading level increases.

The samples cured to 180 °C are substantially cross-linked, and the T_g for pure resin is not detectable. Under these circumstances, one would not expect to see two T_g's, each corresponding to the individual components. After curing at 180 °C, the MSSQ-LO hybrid shows a single, composition-dependent T_g for loading levels ranging from 20 to 70 wt % (Figure 7). Even at 70 wt % loading, the measured T_g is still slightly higher than that of the pure porogen (93 vs 83 °C). The behavior of the MSSQ-HI blends (Figure 6) is somewhat different from that observed for the MSSQ-LO samples. First, an obvious T_g is not detected for the 20 and 30 wt % samples (there is a hint of a transition in the 30 wt % sample). Above these loading levels, a T_g is observed that decreases with increasing loading, although even at 70 wt %, the value is substantially higher than that of the pure porogen (110 vs 83 °C). Here we note that

hybrid samples cured above 125 °C scatter neutrons due to phase separation and pore sizes that increase with loading level are observed upon burnout (TEM and SAXS).[11a,b] In each case, the domains and pore sizes are 3−4 times larger for the MSSQ-LO samples (vide infra). The scattering data suggest that some phase separation does occur at 180 °C for both resins (at least at the higher loading levels >20 wt %) and that the polymer domains are larger for the MSSQ-LO samples.[11a,b,33] This is compared with the MDSC results where the observation of a single composition-dependent T_g is consistent with either the formation of miscible blends or phase separation in systems where the T_g of the matrix is obscured by cross-linking. If the latter interpretation is adopted based on scattering and electron microscopy data, the difference in the MDSC behavior of the MSSQ-LO and MSSQ-HI systems at 180 °C may be attributed to the formation of different domain sizes in each and/or perhaps also to the difference in phase purities. In the next section, we provide fluorescence results to be considered in conjunction with the MDSC, TEM, and scattering studies.

Pyrene Fluorescence in the Hybrid Nanocomposites. Over the past 20 years, fluorescence techniques have provided a powerful tool for obtaining detailed information on miscibility in amorphous polymer−polymer blends[23,24] and on local microenvironments and interfacial interactions in organic−inorganic nanocomposites.[25] Two fluorescence methods have primarily been used to characterize polymer blends. One is nonradiative energy transfer (NRET) developed by Morawetz,[23] in which the excitation energy is transferred from donor to acceptor chromophores provided that the distance between them is of the order of 2−5 nm. The second utilizes excimer fluorescence, an application pioneered by Frank et al.,[24] who took advantage of the fact that excimers are formed in certain aromatic polymers such as polystyrene, poly(2-vinylnaphthalene), poly(1-vinylnaphthalene), and poly(vinylbiphenyl). Excimers are excited-state molecular complexes formed from two structurally identical species, one of which is electronically excited prior to complexation. In the publications on excimer formation in polymers to date, the vast majority have focused on homopolymers or copolymers having pendant aromatic chromophores such as phenyl or naphthyl substituents.

Although excimer fluorescence has been widely employed as a molecular probe of thermodynamic compatibility in solid polymer−polymer blends,[24] there are few examples of its use to probe the miscibility of organic polymer/inorganic polymer nanocomposites.[25] Most of these have focused on composites in which discrete organic molecules are randomly dispersed within the inorganic matrix or on composites in which small organic molecules are linked directly to the inorganic network by covalent bonds. Sol−gel-derived nanocomposite studies have focused primarily on the evolution of solvent concentration, pore structure, dopant dynamics, and homogeneity from the gelation point to the formation of the final solvent-free materials.[26]

One major problem with dispersed hybrid nanocomposites is the difficulty of controlling the precise location of the small molecule fluorescent probe within the matrix due to possible aggregation effects. If low molecular weight probes are simply dispersed in the hybrid nanocomposites, their final locations are determined by the solubility of the probe in either the polymer or the inorganic phase. This problem is mitigated by attaching the chromophores to the polymer molecules (inorganic or organic) by copolymerization or grafting. The direct attachment approach is attractive for development of fluorescence as a general analytical tool for the studies of miscibility in either polymer blends or organic/inorganic nanocomposites. However, a caveat is that the number of fluorophores per polymer chain should be small so that the physical properties of the polymers are not changed. In this paper, the MSSQ resins having different amounts of initial silanol end groups are used to study the effect of end group functionality on the phase separation behavior in hybrid nanocomposites through the measurement of the excimer-to-monomer (I_E/I_M) ratio for a fluorescently tagged organic polymer. This provides a convenient experimental probe of phase separation in the inorganic−polymer hybrid nanocomposites.

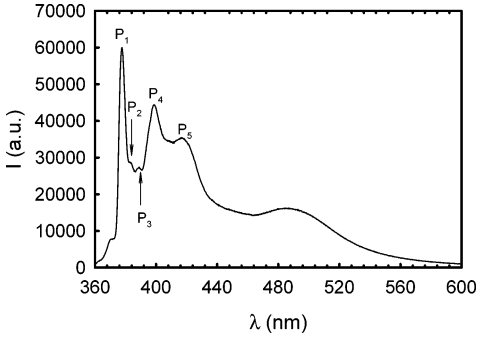

Figure 8. Fluorescence emission spectrum of pure pyrene-labeled P(MMA-*co*-DMAEMA) (λ_{ex} = 343 nm).

Pyrene excimer fluorescence can overcome the insensitivity of the MDSC technique at low porogen loadings and provide an alternative probe of the phase separation behavior in MSSQ/P(MMA-*co*-DMAEMA) hybrid nanocomposites. In principle, this technique can also be used to probe smaller domain sizes than thermal analysis techniques. There are two regions of interest in pyrene emission spectra, as suggested in Figure 8, which shows the film emission spectrum of the pyrene-labeled P(MMA-*co*-DMAEMA). These are (1) the five monomer bands characteristic of the singlet excited pyrene vibronic structure-three distinct peaks (P_1, P_4, and P_5 at 377, 396, and 418 nm) and two shoulders (P_2 and P_3 at 381 and 388 nm) and (2) excimer emission appearing as a broad, structureless band at longer wavelengths (∼480 nm). The formation of pyrene excimers in a polymer below T_g requires the face-to-face distance between an electronically excited and the ground-state pyrene units to be within 4−5 Å with proper orientation.[9a] By measurement of the excimer-to-monomer (I_E/I_M) ratio, we can study the effective local concentration of the fluorophores attached as side chains to the organic polymers.

Figure 9 shows the fluorescence emission spectra of various hybrid nanocomposites formed by py-P(MMA-*co*-DMAEMA) with MSSQ-HI (Figure 9a) and MSSQ-LO (Figure 9b) at different polymer loading levels after curing at 180 °C. Previous thermogravimetric analysis (TGA) studies have verified that the fluorescent polymer is stable to this temperature. All spectra are normalized to the first vibronic band at 377 nm in order to compare the fluorescence behavior of each sample. The broad excimer band at ∼480 nm is obvious in both resin nanocomposites at polymer loading levels above 30 wt %. At very low porogen loading (<5 wt %), essentially

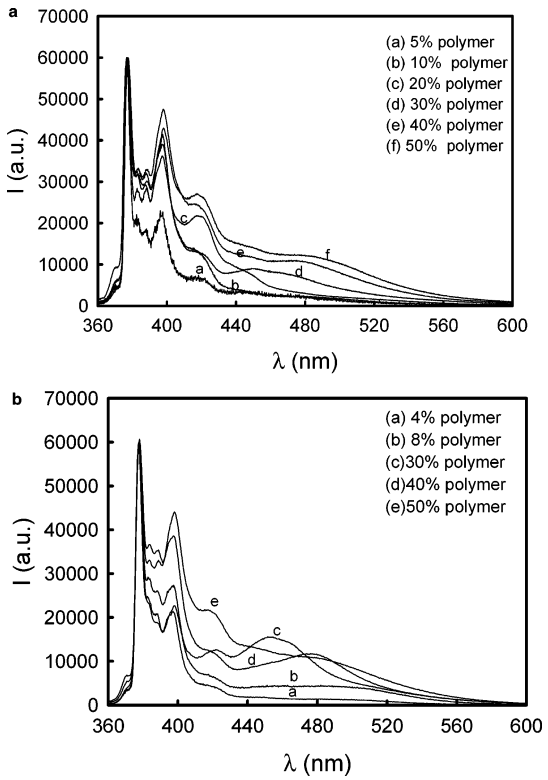

Figure 9. Fluorescence emission spectra of hybrid nanocomposites formed by py-P(MMA-*co*-DMAEMA) with MSSQ-HI (Figure 11a) and MSSQ-LO (Figure 11b) at different polymer loading levels cured at 180 °C.

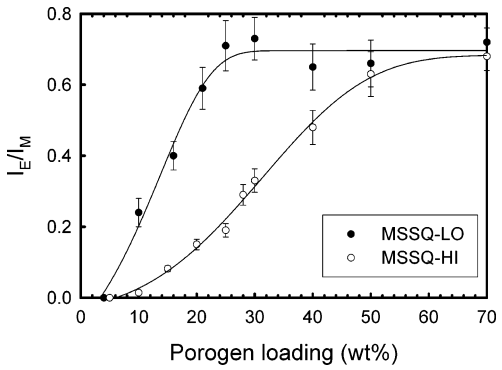

Figure 10. Excimer-to-monomer (I_E/I_M) ratio for nanocomposites formed by py-P(MMA-*co*-DMAEMA) with MSSQ-HI (empty circles) and MSSQ-LO (solid circles) cured at 180 °C. The I_E/I_M ratio for pure py-P(MMA-*co*-DMAEMA) is 0.77.

only the monomer band is observed for both hybrids. In each resin, the relative excimer emission increases with the porogen loading, although it increases much faster for MSSQ-LO samples than for MSSQ-HI hybrids. In addition, the peak position of the broad featureless excimer band red-shifts with increasing porogen loading (e.g., ∼450 nm for 30 wt % vs ∼480 nm for 40 wt % porogen loading), which may be due to the change of the pyrene complex overlapping geometry varying from partial to complete overlap.[16c] The unusual high-energy band position for the excimer in hybrid nanocomposites at 30 wt % porogen loading may be due to constraints on pyrene molecules inside the rigid MSSQ matrixes.

Figure 10 shows the plots of excimer-to-monomer (I_E/I_M) ratio vs porogen loading for nanocomposites formed from py-P(MMA-*co*-DMAEMA) with MSSQ-HI (empty circles) and MSSQ-LO (solid circles) cured at 180 °C. The I_E/I_M ratios used here are peak area ratios calculated from the pyrene emission spectra shown in Figure 9. The monomer peak emission was determined by integrating the peak area from 360 to 430 nm. The excimer peak area was calculated by using either the spectrum of the 5 wt % py-P(MMA-*co*-DMAEMA) in MSSQ-HI hybrid or the 4 wt % py-P(MMA-*co*-DMAEMA) in the MSSQ-LO hybrid as the baseline for area subtraction over the emission range from 430 to 640 nm. Within a py-P(MMA-*co*-DMAEMA) loading range of 4−70 wt %, the I_E/I_M ratio increases gradually with the porogen loading in MSSQ-HI before reaching a plateau at ∼60 wt %. In contrast, it rapidly reaches a plateau at ∼20 wt % for MSSQ-LO. Coincidently, this 20 wt % loading level is close to the measured percolation threshold (closed-cell to open-cell transition) for MSSQ-LO, as determined by positronium annihilation spectroscopy (PAS).[27]

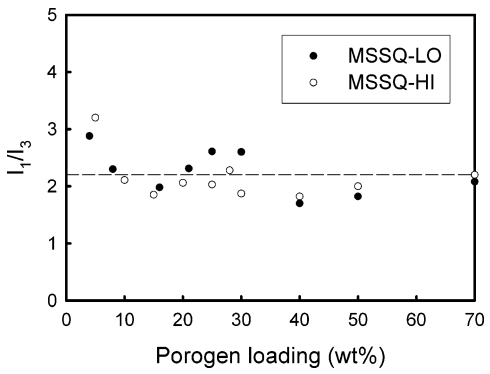

Figure 11. First-to-third peak intensity (I_1/I_3) ratio for nanocomposites formed by py-P(MMA-*co*-DMAEMA) and MSSQ-HI (empty circles) and MSSQ-LO (solid circles) cured at 180 °C. The solid line is used to guide the eye.

The intensities of the vibronic bands in the pyrene monomer emission are known to be strongly dependent on the microenvironment.[18] More specifically, the intensity ratio between the first and third peaks (I_1/I_3) reflects the local polarity surrounding the chromophores and decreases with decreasing environmental polarity.[18] The I_1 peak, ascribed to the 0−0 transition from the lowest electronically excited state to the lowest ground state, is a "symmetry-forbidden" transition that can be enhanced by the distortion of the π-electron cloud (polar environment). On the other hand, the I_3 transition is not symmetry-forbidden and thus is relatively solvent-insensitive. The observed I_1/I_3 ratio of pyrene itself ranges from ∼0.5 in nonpolar solvents such as hexane to about 1.8 in highly polar solvents such as methanol.[18] However, substitution on the aromatic group intrinsically distorts the symmetry and hence decreases the probability of 0−0 transitions.

Although the extent of solvent enhancement of the I_1/I_3 ratio for 1-substituted pyrenes is reduced compared to the unsubstituted pyrene, the I_1/I_3 ratio is still sensitive to the solvent polarity.[28] It ranges from ∼2.3 in nonpolar hydrocarbons such as heptane or toluene to ∼3.2 in highly polar solvents, still a significant difference. Figure 11 shows the I_1/I_3 ratios for nanocomposites formed by py-P(MMA-*co*-DMAEMA) and MSSQ-HI (solid circles) and MSSQ-LO (empty circles) initially cured at 180 °C. Both the MSSQ-HI and MSSQ-LO hybrid nanocomposites exhibit roughly constant I_1/I_3 ratios clustered around 2.2 at polymer loading levels above 10 wt %. This result suggests that the local environment surrounding the pyrene molecules after

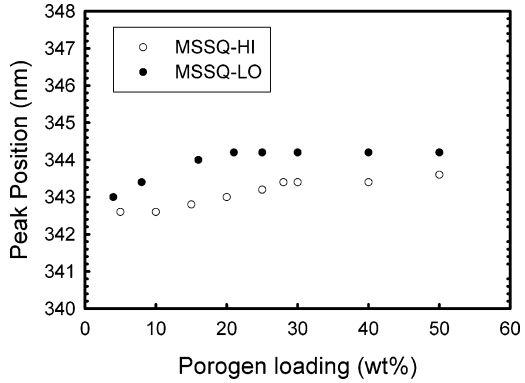

Figure 12. Peak position of the hybrid nanocomposites formed by pyrene-labeled P(MMA-*co*-DMAEMA) with MSSQ-HI (empty circles) and MSSQ-LO (solid circles) cured at 180 °C (λ_{em} = 480 nm).

curing is relatively hydrophobic, except perhaps at the lowest porogen loading. It is interesting that this value is practically identical to that of the pure polymer (~2.2, Figure 8) within the uncertainity of the measurement. The surface hydrophobicity of cured MSSQ nanocomposites, resulting from the condensation of the silanol groups in the MSSQ resins, is also confirmed by contact angle measurements.[29]

Excitation Spectra of Hybrid Nanocomposites. To provide information on the pyrene ground state, we also carried out excitation spectral measurements for nanocomposites formed by py-P(MMA-*co*-DMAEMA) in both MSSQ-HI and MSSQ-LO, as shown in Figure 12. These excitation spectra were monitored at the excimer emission (480 nm). The absorption energy is always higher than that of emission because of internal relaxation of the excited photon to the first excited singlet state. The absorption bands around 375 nm and between 320 and 350 nm originate from transitions from the ^1A ground state of the pyrene ring to the ^1L_b band and the ^1L_a band, respectively.[9a] They correspond to excitation to the first and the second singlet excited states. The ^1L_b band is generally weak because the corresponding transition is symmetry-forbidden, while the ^1L_a bands exhibit relatively higher intensities. Figure 12 shows that the ^1L_a absorption bands initially located at 326 and 343 nm are only slightly red-shifted (0−1.2 nm) upon the addition of py-P(MMA-*co*-DMAEMA) to either MSSQ-LO or MSSQ-HI. It is generally accepted that a red shift of at least 1−4 nm is an indication of ground-state association for pyrene molecules, as commonly observed in pyrene-tagged hydrophobically modified polymers in aqueous solutions[16c] and complex formation in polymer−polyelectrolyte solutions.[30] Thus, the small observed ground-state interactions (red shifts of 0−1.2 nm) are negligible for both MSSQ-HI and MSSQ-LO nanocomposites.

Discussion

In organic−inorganic molecular composites and hybrid nanocomposites, it is possible to form an interfacial region or interphase, which is totally different from either of the individual components. The resulting physical properties of these nanocomposites will show a nonlinear behavior that is mainly due to the interfacial interactions when compared with macroscopic composites made of the same components.[25] Chujo et al. have found that nanoscale phase separation in a silica matrix can only be achieved by using components (porogen + resin) that initially strongly interact with each other by hydrogen bonding or other attractive forces:[31] materials lacking strong interactions typically phase separate macroscopically. Thus, to promote high levels of molecular mixing with organosilicate materials prior to curing, it is important to use polymers with groups (e.g., hydrogen bonding) that can interact with the organosilicate end groups present before curing.

Our previous FTIR studies showed that strong hydrogen-bonding interactions occur between the −SiOH end groups in MSSQ and the tertiary amino substituents in P(MMA-*co*-DMAEMA) in films at 25 °C.[15] Thus, MSSQ and P(MMA-*co*-DMAEMA) readily form nanocomposites with complete mixing at low temperature as evidenced by the observation of a single, composition-dependent T_g by MDSC as shown in Figures 4 and 5 and the absence of significant neutron scattering prior to curing.[11a] The formation of P(MMA-*co*-DMAEMA) domains in an MSSQ matrix is governed by the thermodynamics of phase separation in a two-component system as well as by related kinetic factors before and during the matrix cross-linking. Depending on miscibility, loading level, and processing conditions, phase separation may produce either isolated domains of various sizes via nucleation and growth or interconnected domains through spinodal decomposition. Figure 13 depicts an idealized schematic representation of phase separation in a hybrid system proceeding by a nucleation and growth mechanism. The *Y*-axis represents the degree of cross-linking of a thermosetting matrix material. Assuming the porogen and matrix prepolymer are miscible prior to cross-linking, one can see that phase separation will occur at a lower cross-linking level as the volume fraction of the porogen increases. If phase separation occurs after significant cross-linking, the growth of the initially small domains will be kinetically arrested by the high viscosity of the cross-linked medium, resulting in a nanoscopic hybrid and eventually a porous material with small pores after burnout. If, on the other hand, phase separation begins prior to significant cross-linking, diffusion and coalescence will take place, resulting in larger domains and hence larger pores after burnout. The point at which phase separation occurs depends on many things, including porogen loading level and molecular weight, resin functionality, etc. For the formation of small kinetically arrested domains, ideally the two components should be miscible over a wide concentration range prior to cross-linking, and the resin should begin to cross-link at relatively low temperatures. In the systems studied here, the MSSQ-HI resin has a high concentration of SiOH end groups prior to cross-linking that interact strongly with the porogen,[15] promoting improved miscibility. At the same time, the cross-linking temperature is lower than that of the MSSQ-LO resin (Figure 2) due to the reactivity of the silanol groups. This combination of features would suggest that the MSSQ-HI/P(MMA-*co*-DMAEMA) combination would be expected to produce smaller domains in the hybrid and smaller pores upon burnout than the combination of MSSQ-LO and the porogen. This is indeed the case, as demonstrated by Figure 14, which shows the bright field transmission electron microscopy (TEM) images of nanoporous MSSQ-LO and MSSQ-HI containing 35 wt % polymer initially. TEM results reveal that the average pore size in MSSQ-LO is significantly larger than that

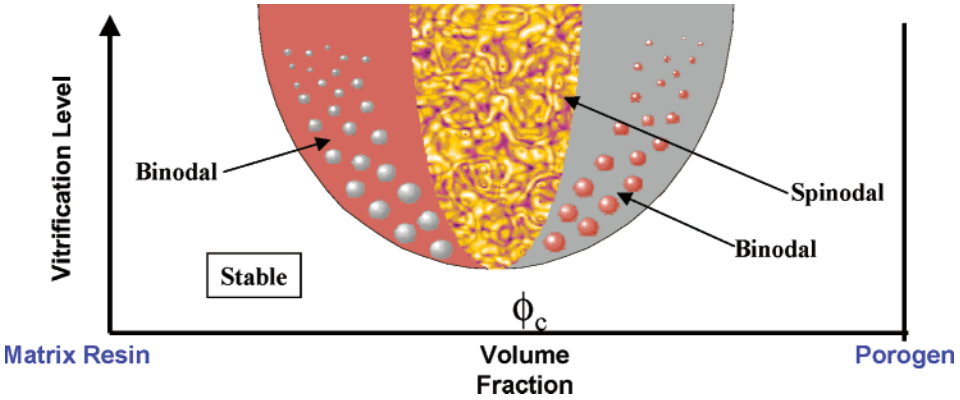

Figure 13. Idealized phase diagram of MSSQ/porogen hybrid nanocomposites as a function of porogen and degree of matrix resin cross-linking.

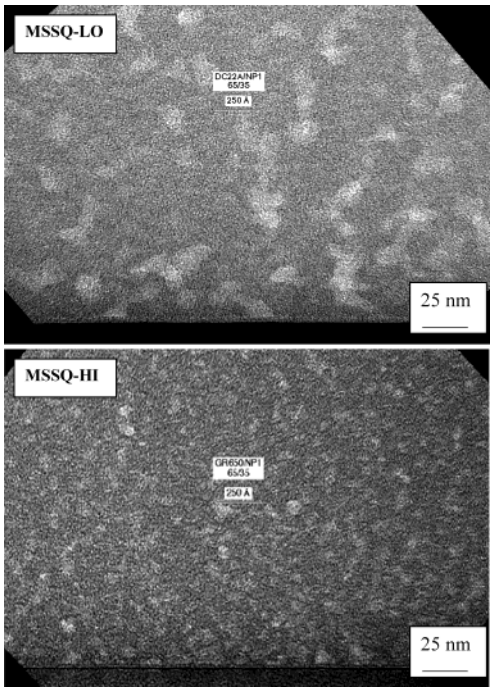

Figure 14. Bright field transmission electron microscopy (TEM) images of the nanoporous MSSQ-LO (top) and MSSQ-HI (bottom) with 35 wt % polymer content initially.

in MSSQ-HI, consistent with our previous SAXS results.[15,33]

Over the past 20 years pyrene excimer fluorescence has proved to be a valuable probe of polymer−polymer miscibility.[24] We have demonstrated here that the same approach is also applicable to the miscibility of organic−inorganic hybrid nanocomposites. In solution, an excimer may form between an electronically excited aromatic ring and an adjacent ground-state ring, which can adopt a coplanar sandwich arrangement because of polymer backbone motions occurring during the lifetime of the excited state. In rigid media such as the cured MSSQ hybrid nanocomposites, on the other hand, segmental motion is restricted so that suitable excimer-forming sites (EFS) occur only between two aromatic rings normally situated in a preexisting sandwich-like arrangement. Although the number of such EFS is relatively small, their influence can be enhanced by the occurrence of energy migration, which funnels the energy absorbed at an isolated ring along the polymer chain into the EFS providing the pyrene concentration is high enough.[32]

The occurrence of phase separation of a fluorescent polymer from a nonfluorescent matrix causes additional intermolecular EFS and may increase the efficiency of the energy migration process as well. Both factors increase the observed excimer fluorescence. A phase-separated system therefore will have a larger value of the ratio of excimer (I_E) to monomer (I_M) fluorescence intensities than a miscible composite of the same bulk composition because of the increased chromophore densities in the former. In a phase-separated system, most of the chromophores will be located in the polymer-rich phase, so that the value of I_E/I_M will be higher. In the case of complete phase separation, the ratio should approach that of the neat polymer. The larger value of the I_E/I_M ratio for MSSQ-LO than MSSQ-HI at any given loading level, as shown in Figure 10, thus indicates that polymer is locally more concentrated in labeled porogen. This may be a result of the formation of larger polymer domains in MSSQ-LO (earlier phase separation and higher phase purities). This result is consistent with our earlier small-angle X-ray scattering (SAXS) data, in which we showed that the final pore size upon burnout for MSSQ-LO is about 4 times larger than that of MSSQ-HI when the initial porogen loading levels were comparable.[15] The rapid saturation of the I_E/I_M ratio at py-P(MMA-*co*-DMAEMA) loading levels above 20 wt % for MSSQ-LO hybrids indicates that the I_E/I_M ratio is apparently not sensitive to polymer domain sizes larger than ∼4−5 nm (vide infra). The understanding of the phase separation behavior of MSSQ/polymer hybrid nanocomposites by photophysical approaches can be further enhanced by small-angle neutron scattering (SANS) using partially deuterated P(MMA-*co*-DMAEMA) of similar molecular weight.[11a] Previous SANS data on MSSQ-LO/P(MMA-*co*-DMAEMA) indicate that the polymer domain sizes progressively increase with loading level (4.6 nm, 20 wt %; 6.2 nm, 30 wt %; highly interconnected spinodal-like structure with a domain spacing 23 nm, 40 wt %).[11a] A weaker scattering intensity at higher q region was observed from more recent SANS studies on MSSQ-HI/P(MMA-*co*-DMAEMA) with 30 wt % P(MMA-*co*-DMAEMA) cured at 180 °C, suggesting smaller and more phase-mixed polymer domains.[11b] Here, we assume that the resulting polymer domain sizes will not be changed by the presence of 3 mol % pyrene moieties in the porogen. We should emphasize that a critical polymer domain size of ∼5 nm exists beyond which the pyrene excimer fluorescence technique loses its sensitivity. A similar saturation point of the I_E/I_M ratio at a py-P(MMA-*co*-

DMAEMA) loading level of ~60 wt % for MSSQ-HI nanohybrid (see Figure 10) also occurs at the polymer domain size of ~5 nm, as determined by SAXS.[15,33] The SAXS studies were done on porous samples after burnout since the porous morphology reflects that of the precursor hybrid.

Summary

In summary, cross-linked MSSQ/P(MMA-*co*-DMAEMA) hybrid nanocomposites, in which the polymer domain structures simulate the final pore morphology upon burnout, were examined using MDSC and excimer fluorescence. We have covalently attached pyrene probe molecules to the non-nitrogeneous methacrylate monomer side chain in P(MMA-*co*-DMAEMA) copolymer at a 3 mol % level. Two different resins, MSSQ-HI and MSSQ-LO, each with different amounts of initial silanol end groups, were used to study the effect of silanol concentration on the phase separation behavior of the hybrid nanocomposites. Our MDSC results show the existence of a single, composition-dependent glass transition temperature for P(MMA-*co*-DMAEMA) at loading levels up to 70 wt % for both MSSQ-HI and MSSQ-LO, which is an indication of the apparent miscibility at the length scale of 10 nm and above at a curing temperature of 80 °C. Pyrene excimer fluorescence, which occurs when an electronically excited-state pyrene approaches within about 4 Å of a ground-state pyrene in a proper geometry, provides an alternate probe of the hybrid nanocomposites formed with MSSQ and pyrene-tagged P(MMA-*co*-DMAEMA). The pyrene fluorescence results show that, for loading levels ranging from 4 to 50 wt % in MSSQ-HI, the I_E/I_M ratio increases gradually with the porogen loading for MSSQ-HI before reaching a plateau at ~60 wt %. In contrast, it reaches a plateau rapidly at ~20 wt % for MSSQ-LO. The larger value of the I_E/I_M ratio for MSSQ-LO at all loading levels surveyed compared to that for MSSQ-HI at the same polymer loading may indicate the formation of larger polymer domains and/or ones of higher phase purity. This result is consistent with TEM results and our previous SAXS data. However, the application of pyrene excimer fluorescence is limited by the fact that it is not sensitive to hybrid nanocomposites with polymer domain size larger than ~5 nm, as determined by SANS or SAXS.

Acknowledgment. This work was supported by the NIST Advanced Technology Program (Contract No. 70NANB8H4013). We thank Dow Corning Corp. for the preparation of the MSSQ-LO samples.

Supporting Information Available: Syntheses of 4-(1′-pyrenebutyl) methacrylate and pyrene-labeled P(MMA-*co*-DMAEMA) and ^{1}H NMR spectrum and GPC traces of py-P(MMA-*co*-DMAEMA). This material is available free of charge via the Internet at http://pubs.acs.org.

References and Notes

(1) (a) Chujo, Y. *Curr. Opin. Solid-State Mater. Sci.* **1996**, *1*, 806. (b) Giannelis, E. P. *Adv. Mater.* **1996**, *8*, 29. (c) Arkles, B. *CHEMTECH* **1999**, *29*, 7. (d) Mascia, L. *Trends Polym. Sci.* **1995**, *3*, 61. (e) Loy, D. A.; Shea, K. J. *Chem. Rev.* **1995**, *95*, 1431. (f) *Better Ceramics Through Chemistry VI: Organic/Inorganic Hybrid Materials*; Coltrain, B. K., Sanchez, C., Schaefer, D. W., Wilkes, G. L., Eds.; *Mater. Res. Soc. Symp. Proc.* **1996**, 435. (g) *Organic/Inorganic Hybrid Materials*; Laine, R. M., Sanchez, C., Brinker, C. J., Giannelis, E., Eds.; *Mater. Res. Soc. Symp. Proc.* **1998**, 519. (h) *Organic/Inorganic Hybrid Materials II*; Klein, L. C., Francis, L. F., DeGuire, M. R., Mark, J. E., Eds.; *Mater. Res. Soc. Symp. Proc.* **1999**, 576. (i) *Organic/Inorganic Hybrid Materials-2000*; Laine, R. M., Sanchez, C., Giannelis, E., Brinker, C. J., Eds.; *Mater. Res. Soc. Symp. Proc.* **2001**, 628.

(2) (a) Miller, R. D. *Science* **1999**, *286*, 421. (b) Maier, G. *Prog. Polym. Sci.* **2001**, *26*, 3. (c) Nguyen, C. N.; Carter, K. R.; Hawker, C. J.; Hedrick, J. L.; Jaffe, R. L.; Miller, R. D.; Remenar, J. F.; Rhee, H.-W.; Rice, P. M.; Toney, M. F.; Trollsås, M.; Yoon, D. Y. *Chem. Mater.* **1999**, *11*, 3080. (d) Hedrick, J. L.; Miller, R. D.; Hawker, C. J.; Carter, K. R.; Volksen, W.; Yoon, D. Y.; Trollsås, M. *Adv. Mater.* **1998**, *10*, 1049. (e) Nguyen, C. N.; Hawker, C. J.; Miller, R. D.; Huang, E.; Hedrick, J. L.; Gauderon, R.; Hilborn, J. G. *Macromolecules* **2000**, *33*, 4281.

(3) (a) Rottman, C.; Grader, G.; DeHazan, Y.; Melchior, S.; Avnir, D. *J. Am. Chem. Soc.* **1999**, *121*, 8533. (b) Dantas de Morais, T.; Chaput, F.; Bailot, J.-P.; Lahlil, K.; Darracq, B.; Levy, Y. *Adv. Mater.* **1999**, *11*, 107.

(4) (a) Lev, O.; Tsionsky, M.; Rabinovich, L.; Glezer, V.; Sampath, S.; Pankratov, I.; Gun, J. *Anal. Chem.* **1995**, *67*, 22A. (b) Harmer, M. A.; Farneth, W. E.; Sun, Q. *J. Am. Chem. Soc.* **1996**, *118*, 7708. (c) Schubert, U. *New J. Chem.* **1994**, *18*, 1049.

(5) (a) Guizard, C.; Lacan, P. *New J. Chem.* **1994**, *18*, 1097. (b) Smaihi, M.; Jermoumi, T.; Marignan, J.; Noble, R. D. *J. Membr. Sci.* **1996**, *116*, 211.

(6) (a) Beecroft, L. L.; Ober, C. K. *Chem. Mater.* **1997**, *9*, 1302. (b) Klein, L. C. *Sol−gel Optics, Processing and Applications*; Kluwer: Boston, 1994. (c) Sanchez, C.; Lebeau, B. *MRS Bull.* **2001**, *26*, 377.

(7) (a) Brinker, C. J.; Scherer, G. W. *Sol−gel Science: The Physics and Chemistry of Sol−Gel Processing*; Academic Press: San Diego, 1990. (b) Hench, L. L.; West, J. K. *Chem. Rev.* **1990**, *90*, 33.

(8) *Handbook of Multilevel Metallization of Integrated Circuits*; Wilson, S. R., Tracy, C. J., Freeman, J. L., Jr., Eds.; Noyes Publications: Park Ridge, NJ, 1993.

(9) (a) Birks, J. B. *Photophysics of Aromatic Molecules*; Wiley-Interscience: New York, 1970. (b) Lakowicz, J. R. *Principles of Fluorescence Spectroscopy*, 2nd ed.; Plenum Press: New York, 1999.

(10) (a) Lin, T. S.; Ward, T. C. *Polym. Prepr.* **1983**, *24* (2), 136. (b) Clauss, J.; Schmidtrohr, K.; Spiess, H. W. *Acta Polym.* **1993**, *44*, 1. (c) VanderHart, D. L.; McFadden, G. B. *Solid State Nucl. Magn. Reson.* **1996**, *7*, 45. (d) Bauer, F.; Ernst, H.; Decker, U.; Findeisen, M.; Flasel, H.-J.; Langguth, H.; Hartmann, E.; Mehnert, R.; Peuker, C. *Macromol. Chem. Phys.* **2000**, *201*, 2654.

(11) (a) Yang, G. Y.; Briber, R. M.; Huang, E.; Rice, P. M.; Volksen, W.; Miller, R. D. *Polym. Mater. Sci. Eng.* **2001**, *85*, 18. (b) Kim, H.-C.; Lin, Z.; Ahn, S.; Briber, R. M.; Miller, R. D. Work in preparation. (c) Higgins, J. S.; Benoit, H. C. *Polymers and Neutron Scattering*; Oxford University Press: Oxford, England, 1996. (d) Dahmouche, K.; Santilli, C. V.; Pulcinelli, S. H.; Craievich, A. F. *J. Phys. Chem. B* **1999**, *103*, 4937. (e) Rodrigues, D. E.; Brennan, A. B.; Betrabet, C.; Wang, B.; Wilkes, G. L. *Chem. Mater.* **1992**, *4*, 1437.

(12) (a) Chen, T. K.; Tien, Y. L.; Wei, K. H. *Polymer* **2000**, *41*, 1345. (b) Lee, A.; Lichtenhan, J. D. *J. Appl. Polym. Sci.* **1999**, *73*, 1993.

(13) (a) Young, S. K.; Mauritz, K. A. *J. Polym. Sci., Part B: Polym. Phys.* **2001**, *39*, 1282. (b) Shelley, J. S.; Mather, P. T.; DeVries, K. L. *Polymer* **2001**, *42*, 5849. (c) Suh, D. J.; Lim, Y. T.; Park, O. O. *Polymer* **2000**, *41*, 8557.

(14) (a) Anastasiadis, S. H.; Karatasos, K.; Vlachos, G.; Manias, E.; Giannelis, E. P. *Mater. Res. Soc. Symp. Proc.* **1999**, *543*, 125. (b) Anastasiadis, S. H.; Karatasos, K.; Vlachos, G.; Manias, E.; Giannelis, E. P. *Phys. Rev. Lett.* **2000**, *84*, 915.

(15) Huang, Q. R.; Volksen, W.; Huang, E.; Toney, M.; Frank, C. W.; Miller, R. D. *Chem. Mater.* **2002**, *14*, 3676.

(16) (a) Semerak, S. N.; Frank, C. W. *Adv. Polym. Sci.* **1983**, *54*, 31. (b) Dong, D. C.; Winnik, M. A. *Can. J. Chem.* **1985**, *62*, 2560. (c) Winnik, F. M. *Chem. Rev.* **1993**, *93*, 587.

(17) Semerak, S. N.; Frank, C. W. *Adv. Chem. Ser.* **1983**, *203*, 751.

(18) (a) Kalyanasundaram, K.; Thomas, J. K. *J. Am. Chem. Soc.* **1977**, *99*, 2039. (b) Nakajima, A. *Bull. Chem. Soc. Jpn.* **1971**, *44*, 3272.

(19) Dreezen, G.; Groeninckx, G.; Swier, S.; Van Mele, B. *Polymer* **2001**, *42*, 1449.

(20) Inoue, T. *Prog. Polym. Sci.* **1995**, *20*, 119.

(21) (a) Utracki, L. A. *Polymer Alloys and Blends*; Munich: Hanser, 1989. (b) Guo, M. *Trends Polym. Sci.* **1996**, *4*, 238.

(22) (a) Carter, K. R.; Cook, R. F.; Harbison, M. A.; Hawker, C. J.; Hedrick, J. L.; Kim, S. M.; Liniger, E. G.; Miller, R. D.; Volksen, W.; Yoon, D. Y. U.S. Patent 5,953,627, 1999. (b) Carter, K. R.; Cook, R. F.; Harbison, M. A.; Hawker, C. J.; Hedrick, J. L.; Lee, V. Y.; Liniger, E. G.; Miller, R. D.; Volksen, W.; Yoon, D. Y. U.S. Patent 6,177,360 B1, 2001.

(23) (a) Morawetz, H. *Polym. Sci. Eng.* **1983**, *23*, 689. (b) Morawetz, H.; Amrani, F. *Macromolecules* **1978**, *11*, 281. (c) Morawetz, H. *Ann. N.Y. Acad. Sci.* **1981**, *366*, 404.

(24) (a) Frank, C. W.; Gashgari, M. A. *Macromolecules* **1979**, *12*, 163. (b) Frank, C. W.; Gashgari, M. A.; Semerak, S. N. *NATO ASI Ser., Ser. C* **1986**, *182*, 523. (c) Gashgari, M. A.; Frank, C. W. *Macromolecules* **1988**, *21*, 2782. (d) Tao, W. C.; Thomas, J. W.; Frank, C. W. *Polymer* **1988**, *29*, 1625. (e) Frank, C. W.; Zin, W. C. *ACS Symp. Ser.* **1987**, *358*, 18.

(25) (a) Leezenberg, P. B.; Frank, C. W. *Chem. Mater.* **1995**, *7*, 1784. (b) Goda, H.; Frank, C. W. *Chem. Mater.* **2001**, *13*, 2783. (c) Ha, C. S.; Park, H.-D.; Frank, C. W. *Chem. Mater.* **2000**, *12*, 839.

(26) (a) Keeling-Tucker, T.; Brennan, J. D. *Chem. Mater.* **2001**, *13*, 3331. (b) Katz, A.; Davis, M. E. *Nature (London)* **2000**, *403*, 286. (c) Matsui, K.; Nakazawa, T.; Morisaka, H. *J. Phys. Chem.* **1991**, *95*, 976. (d) Kaufman, V. R.; Avnir, D. *Langmuir* **1986**, *2*, 717. (e) Matsui, K.; Nakazawa, T. *Bull. Chem. Soc. Jpn.* **1990**, *63*, 11.

(27) Petkov, M. P.; Weber, M. H.; Lynn, K. G.; Rodbell, K. P.; Volksen, W.; Miller, R. D. *Proc. Mater. Res. Soc.*, in press.

(28) (a) Char, K.; Frank, C. W.; Gast, A. P.; Tang, W. T. *Macromolecules* **1987**, *20*, 1833. (b) Char, K.; Gast, A. P.; Frank, C. W. *Langmuir* **1988**, *4*, 989. (c) Chen, S. H.; Frank, C. W. *Langmuir* **1991**, *7*, 1719.

(29) Huang, Q. R.; Frank, C. W.; Mecerreyes, D.; Miller, R. D. *Polym. Mater. Sci. Eng.* **2001**, *84*, 792.

(30) (a) *Polymers in Aqueous Media*; Glass, J. E., Ed.; Advances in Chemistry Series 223; American Chemical Society: Washington, DC, 1989. (b) Frank, C. W.; Hemker, D. J.; Oyama, H. T. *Water Soluble Polymers*; Glass, J. E., Ed.; Advances in Chemistry Series 213; American Chemical Society: Washington, DC, 1991; Chapter 20.

(31) Chujo, Y.; Saegusa, T. *Adv. Polym. Sci.* **1992**, *100*, 11.

(32) Klöpffer, W. *Spectrosc. Lett.* **1978**, *11*, 863.

(33) Huang, E.; Toney, M. F.; Volksen, W.; Mecerreyes, D.; Brock, P.; Kim, H.-C.; Hawker, C. J.; Hedrick, J. L.; Lee, V. Y.; Magbitang, T.; Miller, R. D.; Lurio, L. B. *Appl. Phys. Lett.* **2002**, *81* (12), 2232.

MA034034D